CONF-810801--58

CONF-810801--58

DE82 005954

OBSERVATIONS OF THE SEVERITY OF NOTCH-ROOT RADIUS IN INITIATION OF SUBCRITICAL CRACK GROWTH

W. G. Reuter, C. R. Eiholzer, M. A. Tupper

HGW

SUMMARY

Slow bend tests were conducted on Charpy specimens containing precracks or machined notches of 0.10 or 0.25 mm radius. The test specimens were fabricated from three heats of annealed Type 304 stainless steel. The purpose of these tests was to examine the effects of notch root radius, in very ductile materials, on initiation of subcritical crack growth. In addition, it was intended to establish the critical values of J, COD, etc. for the single-edge notch specimen for comparison with results obtained from specimens containing surface flaws. This paper will briefly describe only those results of the calculation for J. The tests were monitored by acoustic emission to identify the load corresponding to initiation of subcritical crack growth, by a crack-opening displacement gage (COD), by cross-head displacement, and by stop-action photography.

Previous tests have shown a substantial increase in the notch-root radius prior to initiation of subcritical crack growth. But, tests of the Charpy specimens have shown a negligible increase in notch root radius prior to initiation of subcritical crack growth. But, there was a substantial increase in the notch-root radius prior to attainment of the maximum load. The loads corresponding to initiation of subcritical crack growth are similar for precracked specimens where the ratio of crack depth (a) to specimen depth (w) is 0.23 and machined notch specimens where a/w = 0.20.

Charpy specimens that had fatigue precracks varying from a/w = 0.23 to 0.71 were used to calculate J. The results are higher than those obtained using specimens containing surface flaws. It has not been possible to obtain a value of J_{crit} from the Charpy specimens due to the shape of the plot of J versus deflection and the substantial range of the deflection corresponding to initiation of subcritical crack growth.

ACKNOWLEDGEMENT

This work was performed in the Materials Application Section of the Materials Technology Division at EG&G Idaho, Inc., under the auspices of the U. S. Department of Energy, Office of Energy Research, Office of Basic Energy Sciences, under DOE Contract No. DE-AC07-76ID01570.

Introduction

A continuing program at EG&G Idaho, Inc. is investigating the capabilities of some of the various analytical techniques presently being developed for elastic-plastic fracture analysis. A portion of the work to date has involved testing plate and pipe specimens fabricated from annealed Type 304 SS (stainless steel). These specimens contained surface defects of either rectangular, triangular, or ellipsoidal configuration in the plate and triangular defects located on the inner or outer surface of the pipe. The defects were put in by electric-discharge machining (EDM) and tested without fatigue precracking.

The decision to use the EDM defect as opposed to the fatigue precrack was based on the substantial ductility of the material and on reference [1] where it was suggested that the stress for initiation of a crack is essentially the same for a fatigue crack, an EDM notch, or for a sharp saw cut. Much of this is based on expectations that the considerable ductility exhibited by this type of material will result in substantial blunting. Observations concerning the blunting at the tip of the defect were verified in this study. (Some of the observations are documented in reference [2].) For these tests, the notch root radii were nominally 0.10 mm, in general agreement with reference [1].

Proof was not available as to the adequacy of the EDM defect in simulating a crack. Therefore, a study program was initiated using Charpy V-notch specimens having either a 0.10 or a 0.25-mm radius machined notch or a fatigue precrack. A number of specimens were precracked where each specimen had a different crack length (a) so that a/w, where w = 10.0 mm, varied from 0.23 to 0.71. These specimens were intended to be used to calculate J, based on the approach described in reference [3]. For this paper, only those specimens containing fatigue cracks, where a/w = 0.23, are used for comparison with specimens containing machined notches, where a/w = 0.20.

Specimens were machined from three different heats of annealed Type 304 SS and oriented so that the crack penetrated the thickness in the same manner as the crack in specimens with surface flaws. The specimens were tested in three-point, slow-bend loading. Additional information regarding the specimens containing the surface flaw may be found in references [4-6].

This paper presents documentation of the behavior at the tip of the defect as a function of the initial sharpness. Behavior is characterized by the blunting observed at the crack tip, and a comparison of the loads required to initiate subcritical crack growth. A brief comparison will be made of the results obtained from calculating J from the Charpy specimens containing precracks and the results in reference [6] from specimens containing surface flaws.

2. Data Collection

2.1 Notch Tip Behavior

Instrumentation used to collect test data consisted of a crack-opening displacement (COD) gage, acoustic emission, linear variable differential transformer (LVTD), cross-head displacement, and stop-action photography. The LVTD was used only to evaluate the suitability of the cross-head displacement. Photographs were taken normal to the notch, to permit direct measurements of the radii. At the same time, photographs were also taken at an oblique angle to the notch so information related to initiation of subcritical crack growth and the overall deformation process could be obtained.

Figures 1 and 2 provide examples of some of the photographs taken at normal and oblique angles respectively for specimen 46 with a machined root radius of 0.25 mm. Figures 3 and 4 provide similar examples for specimen 38 with a machined notch root radius of 0.10 mm. Figures 5 and 6 provide similar examples for specimen 45 containing a precrack.

The radius of the notch tip was measured for two specimens (38 and 77) having an initial radius of 0.08 mm and two specimens (46 and 79) having an initial notch root radius of 0.25 mm. The results of these measurements are plotted in Figure 7.

2.2 Initiation of Subcritical Crack Growth

The loads corresponding to initiation of subcritical crack growth are located in Table 1 for specimens containing either a machined notch root radius or a fatigue precrack. The loads corresponding to initiation were detected by acoustic emission techniques where one sensor was mounted directly on the specimen and the second sensor was mounted on the tooling. The acoustic emission system was capable of discriminating between signals originating external or internal to the source of interest. Therefore, it was possible to allow only those signals originating from the source of concern to be transmitted to the data collection system.

3. Discussion of Results

3.1 Notch (Crack)-Tip Behavior

Figure 1 shows that some plastic deformation has occurred at the notch root at 7.78 KN and the notch root radius continues to grow as the load increases to 13.34 KN. The oblique photographs in Figure 2 suggest that the notch is simply being unrolled with a substantial increase in notch root radius. Similar observations may be made for Figures 3 and 4. For Figure 5, however, the crack is starting to open at 5.56 KN, it appears to be blunted at 11.12 KN, and is very sharp at 12.23 KN (specimen unloaded immediately after this photograph was taken). Figure 6 shows the crack opening as a function of increasing load.

As shown in Figures 1-4, there is very little difference between the behavior of specimens with a machined notch root radius of 0.08 or 0.25 mm. In both instances the notch root radius increased substantially throughout the test as shown in Figure 7. Evaluating the radius in Figure 7, at a constant load, for the same heat of material shows a substantial difference of notch root radius as a function of the original radius. In addition, there is a substantial difference in the radius in Figure 7, at a constant load, even when the initial values are the same but for two different heats.

Since specimens 38 and 46 both came from heat 2 and specimens 77 and 79 both came from heat 3, the adverse impact of any differences in material behavior could be reduced by normalization. This was done by dividing the notch root radius of specimen 46 by that of specimen 38 and by dividing the notch root radius of specimen 79 by that of specimen 77. The results of this normalization are shown in Figure 8. Figure 8 suggests that once plastic deformation begins to occur that there is a tendency for the ratio to decrease to a lower constant value. However, this observation is dependent upon which heat is being examined since the apparent limit for heat 2 is 1.5 but for heat 3 is 1.2.

There was very little increase in the notch root radius prior to initiation of subcritical crack growth, which occurred at about 5.5 KN, see Table 1 and Figures 1, 3, 7, and 8. This is inconsistent with the observations made in reference 2 where photographs taken at the maximum depth of the surface flaw showed substantial blunting prior to

...tion of subcritical crack growth. As these comparisons are made of the same material ... with the flaw oriented in the same direction, the only differences are due to: (1) loading, i.e., tension versus bending, (2) a surface flaw as opposed to a single-edge notch configuration, and (3) the difference in thickness of 6.35 mm for the specimens containing a surface flaw and a thickness of 9.91 mm for the Charpy V-notch specimen.

The difference in the notch configuration would be expected to create the reverse observations, e.g., the larger observed radius would be associated with the two-dimensional defect (SEN) as opposed to the three-dimensional defect (surface flaw). In addition, it is expected that this difference in thickness is not consequential for annealed Type 304 SS, although the thicker specimen would encounter more restraint and would be expected to exhibit a smaller plastic zone size. Therefore, it appears that the observed differences are probably due to the type of loading. This suggests that the bending type of loading which applies the maximum stress at the outer edge of the specimen with a substantial stress gradient through the thickness may provide the explanation.

A microhardness traverse was conducted on specimen 38 prior to and after being tested. These results are shown in Figure 9; a comparison with Figure 10 of Reference 2 shows a very similar behavior in the hardness achieved as well as in the depth of the increased hardness. Neither the above results nor the oblique photographs in Figures 2 and 4 provide any suggestions as to the minimal amount of blunting, prior to initiation of subcritical crack growth, at the notch root. The notch root finally achieved a radius similar to that observed in Reference 2 after being loaded to in excess of 8.90 KN. By this time a substantial amount of cracking had occurred.

There is considerable similarity in behavior of specimens containing a precrack and those containing a machined notch. Some blunting was observed for the fatigue crack, see Figure 5c. The extent of the blunting is much less than that observed for the specimens containing the machined notch. Note in Figure 5d the crack is again sharp. There is some crack growth apparent in Figures 6a-d, but it is obvious that the crack-tip opening displacement is substantial, see also Figures 5c and d. The appearance of the crack in Figure 5c suggests some misalignment of the specimen which appears to be within tolerance in Figure 5a.

3.2 Initiation of Subcritical Crack Growth

An examination of Table 1 shows that the loads corresponding to initiation of subcritical crack growth are essentially the same for the specimens having either a 0.10- or 0.25-mm machined notch root radius with the exception of heat 3. At this time it is not possible to explain the apparent anomalous behavior for heat 3 specimens containing the 0.25-mm machined notch. The anomaly is not that the load, corresponding to initiation of subcritical crack growth for specimens with a notch root radius of 0.25 mm, is much lower in heat 3 than in either heat 1 or 2; but in that the same behavior was not also observed for specimens with a notch root radius of 0.10 mm.

The loads corresponding to initiation of subcritical crack growth are generally similar for precracked specimens with a/w = 0.23 and notched specimens where a/w = 0.20 as shown in Table 1. One possible explanation in the similarity in behavior may be attributed to the work hardening that occurred during the fatigue cracking. Therefore, a series of microhardness traverses were taken from the notch root or the end of the fatigue crack. Readings were taken at 0.25-mm intervals and proceed in the direction of crack growth. The

results indicate a maximum hardness of R_B 98 whereas the general base material has R_B 90. The higher hardness values decrease in about 0.76 mm to the nominal value. The specimens that have been fatigue cracked have only slightly higher hardness at the tip than was measured at the notch root on the specimen with the machined notch.

Another parameter that needs to be evaluated is the acoustic emission system. Even though acoustic emission detected the onset of subcritical crack growth, it is necessary to evaluate what was being detected. This is necessary because an increase in sensitivity will cause the system to generally detect initiation at a lower load. It was, however, possible to verify that cracking had occurred, in the Charpy specimen, at the load of 6.67 KN which exceeds the loads in Table 1, corresponding to initiation of cracking. This was done by loading five specimens from heat 2, each having a machined notch root radius of 0.10 mm. The tests were designed so that the load was terminated at 6.67 KN for specimen 59, at 8.90 KN for specimen 47, at 11.12 KN for specimen 44, at 15.57 KN for specimen 50, and 20.02 KN for specimen 35. As shown in Table 1, the loads corresponding to initiation of subcritical crack growth for specimens 59, 47, and 44 were 6.38, 5.78, and 5.94 KN respectively. Photomicrographs taken of the notch root radius are shown in Figure 10. Specimen 56 has not been exposed to any load and is used as an example of the notch root radius prior to application of a load.

From Figure 10 it is apparent that very fine cracks and holes are visible in Figures 10b and 10c for specimen 59. As the loading for specimen 59 was terminated at 6.67 KN but acoustic emission detected onset of subcritical crack growth at 6.38 KN, there appears to be general agreement. Specimen 56 in Figure 10a shows that neither holes nor cracks of the type observed in Figures 10b and c are visible. This observation suggests that the cracks and holes observed in specimen 59 are indeed due to the testing and were probably the type of items detected by acoustic emission. Figure 10d shows that considerable cracking has occurred by the time the specimen is loaded to 8.90 KN.

The Charpy specimens that had fatigue cracks varying from a/w = 0.23 to 0.71 were used to calculate J based on the approach in reference [3]. The results were similar, but higher than that shown in Figure 8 of reference [6]. The plot of J versus deflection did not flatten out for any specific value of J which might be identified as J_{crit}. An evaluation of the deflections corresponding to initiation of subcritical crack growth found them to vary from 0.5 to 2.5 mm where the corresponding values of J_{crit} would vary from 0.1 to 2.3 MJ/m^2.

REFERENCES

[1] Kanninen, M. F., et al, Mechanical Fracture Predictions for Sensitized Stainless Steel Piping With Circumferential Cracks, EPRI NP-192, Electric Power Research Institute,

[2] Reuter, W. G., Place, T. A., and Brown, H. L., "Mechanism of Initiation, Subcritical Crack Growth and Instability for Annealed Type 304 Stainless Steel," Engineering Fracture Mechanics, accepted for publication.

[3] Begley, J. A., and Landes, J. D., "The J Integral as a Fracture Criterion," Fracture Toughness, Proceedings of the 1971 National Symposium on Fracture Mechanics, Part II, ASTM STP 514, American Society for Testing and Materials, 1972, pp. 1-20.

[4] Reuter, W. G., and Place, T. A., "Using an Equation Based on Flow Stress to Estimate Structural Integrity of Annealed Type 304 Stainless Steel Plate and Pipes Containing

Surface Defects," International Journal of Pressure Vessels and Piping, accepted for publication.

[5] Reuter, W. G., and Place, T. A., "Estimating Structural Integrity, Using the TPFC Approach, of Annealed Type 304 Stainless Steel Plate and Pipes Containing Surface Defects," submitted for publication to the International Journal of Pressure Vessels and Piping.

[6] Reuter, W. G., "Evaluation of the Capabilities of Various Analytical Techniques to Predict Integrity of Structural Components Containing Surface Flaws," Paper F 7/1, Proc. Sixth International Conference on Structural Mechanics in Reactor Technology, Paris, France, August 1981.

TABLE 1. LOAD CORRESPONDING TO INITIATION OF SUBCRITICAL CRACK GROWTH

Heat No.	Root Radius (mm)	Specimen Number	Load at Crack Initiation (Newtons)	Average (Range)
1	0.250	13	5.7×10^3	5.4×10^3 ($4.7 - 5.7$)
		19	5.7×10^3	
		28	4.7×10^3	
	0.100	2*	20×10^3	
		5*	12.4×10^3	
		8	5.0×10^3	5.6×10^3 ($5.0 - 6.3$)
		17	5.5×10^3	
		20	6.3×10^3	
	a/w = 0.24	21	7.3×10^3	
2	0.250	31	6.2×10^3	5.9×10^3 ($5.4 - 6.2$)
		55	6.2×10^3	
		58	5.4×10^3	
	0.100	32	5.4×10^3	5.3×10^3 ($4.3 - 6.2$)
		35	6.2×10^3	
		44	5.9×10^3	
		47	5.7×10^3	
		50	4.3×10^3	
		59	4.3×10^3	
	a/w = 0.24	57	6.1×10^3	
3	0.250	73	3.4×10^3	3.2×10^3 ($3.1 - 3.4$)
		76	3.1×10^3	
		85	3.1×10^3	
	0.100	62	4.5×10^3	6.3×10^3 ($4.5 - 7.5$)
		74	6.3×10^3	
		80	7.5×10^3	
		89	6.8×10^3	
	a/w = 0.23	70	6.6×10^3	

* Results appear anomalous, but the reason has not yet been determined.

Figure 1. Normal view of slow-bend test of Specimen 46 (0.25-mm notch root radius).

(a) At 6.67 KN.

(b) At 7.78 KN.

(c) At 11.12 KN.

(d) At 13.34 KN.

Figure 2. Oblique view of slow-bend test of Specimen 46 (0.25-mm notch root radius).

(a) At 6.67 KN.

(b) At 7.78 KN.

(c) At 11.12 KN.

(d) At 13.34 KN.

Figure 3. Normal view of slow-bend test of Specimen 38 (0.10-mm notch root radius).

(a) At 5.56 KN.

(b) At 7.78 KN.

(c) At 11.12 KN.

(d) At 13.34 KN.

Figure 4. Oblique view of slow-bend test of Specimen 38 (0.10-mm notch root radius).

(a) At 5.56 KN.

(b) At 7.78 KN.

(c) At 11.12 KN.

(d) At 13.34 KN.

Figure 5. Normal view of slow-bend test of Specimen 45 (precracked, a/w = 0.23).

(a) At 5.56 KN.

(b) At 7.78 KN.

(c) At 11.12 KN.

(d) At 12.23 KN.

Figure 6. Oblique view of slow-bend test of Specimen 45 (precracked, a/w = 0.23)

(a) At 5.56 KN.

(b) At 7.78 KN.

(c) At 11.12 KN.

(d) At 12.23 KN.

Figure 7. Plot of notch root radius versus applied load.

Figure 8. Plot of the ratio of large radius to small radius versus applied load.

Figure 9. Plot of hardness versus distance from tip of crack or machined notch for Specimen 38.

Figure 10. SEM photographs of the notch tip region for three different specimens.

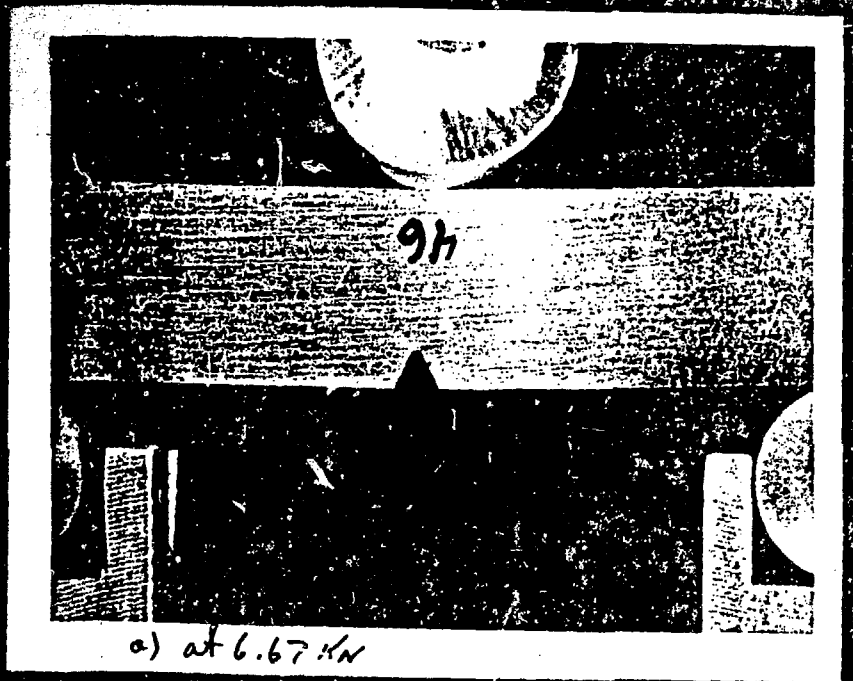

a) at 6.67 KN

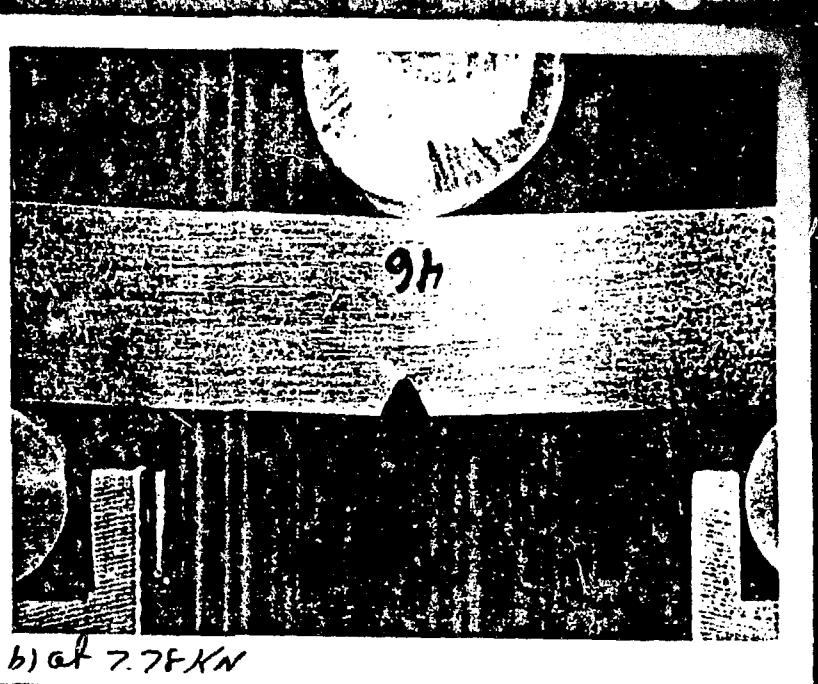

b) at 7.78 KN

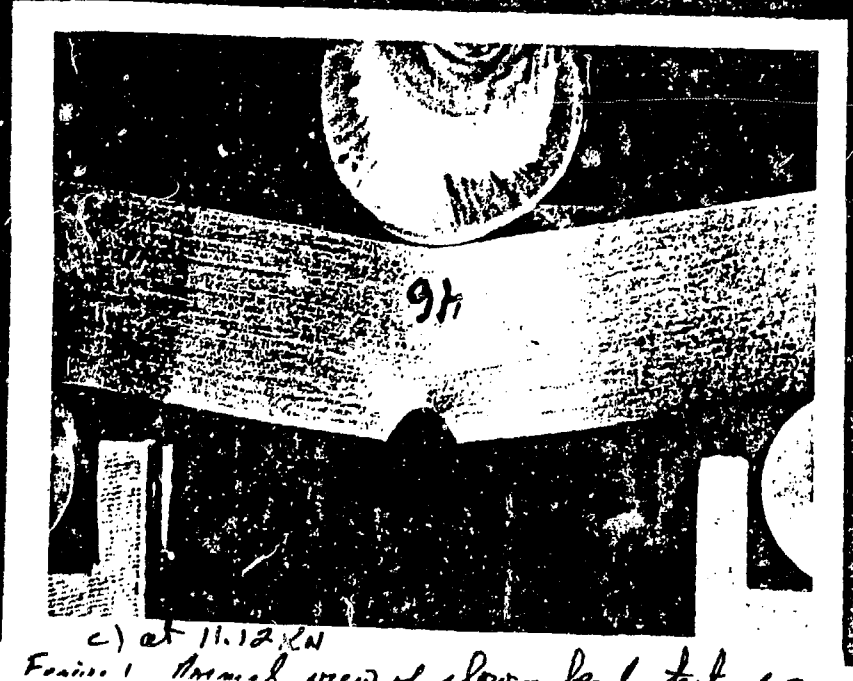

c) at 11.12 KN

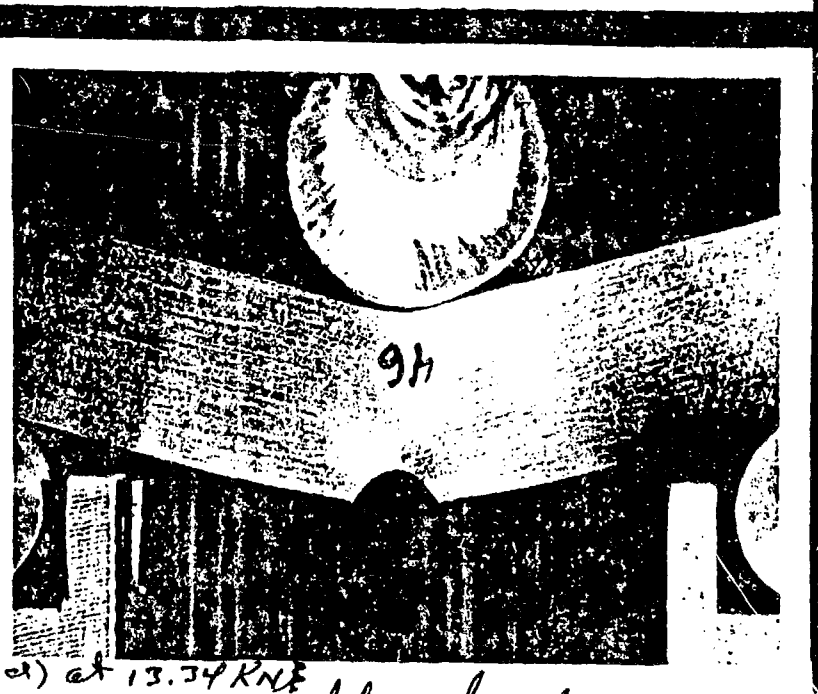

d) at 13.34 KN

Fig. 1 Normal crack at slow-bend test of specimen 46 (0.25-mm notch root radius)

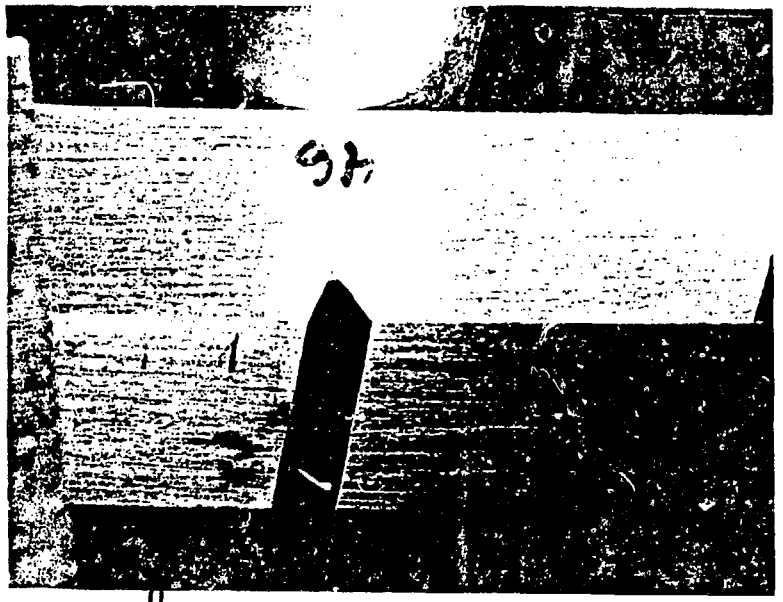

a) at 6.67 KN

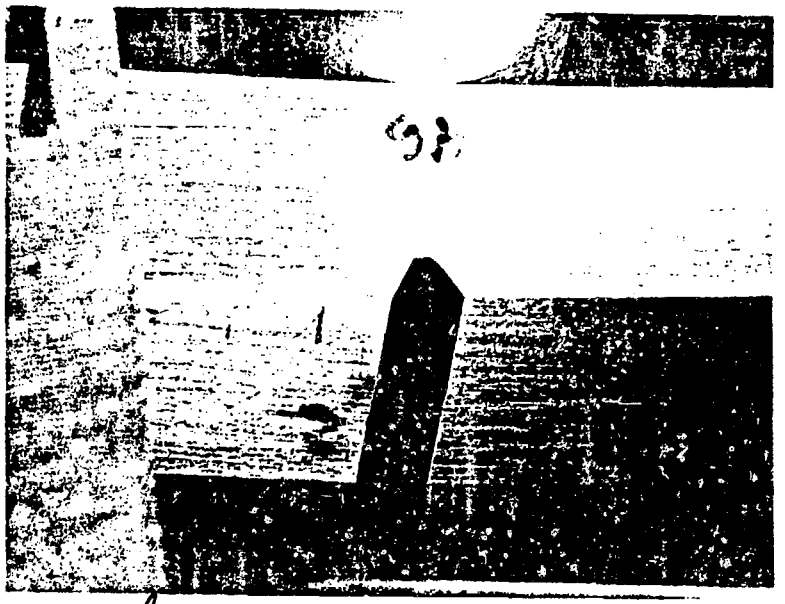

b) at 7.74 KN

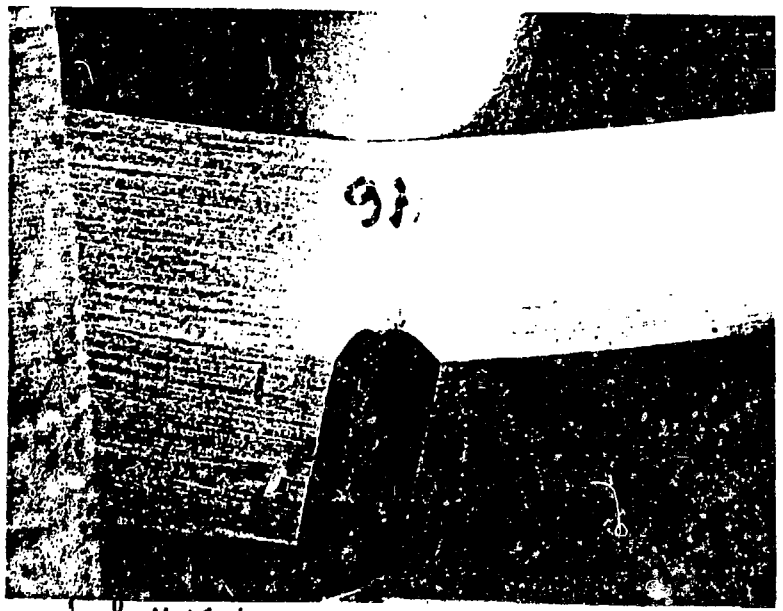

c) at 11.12 KN

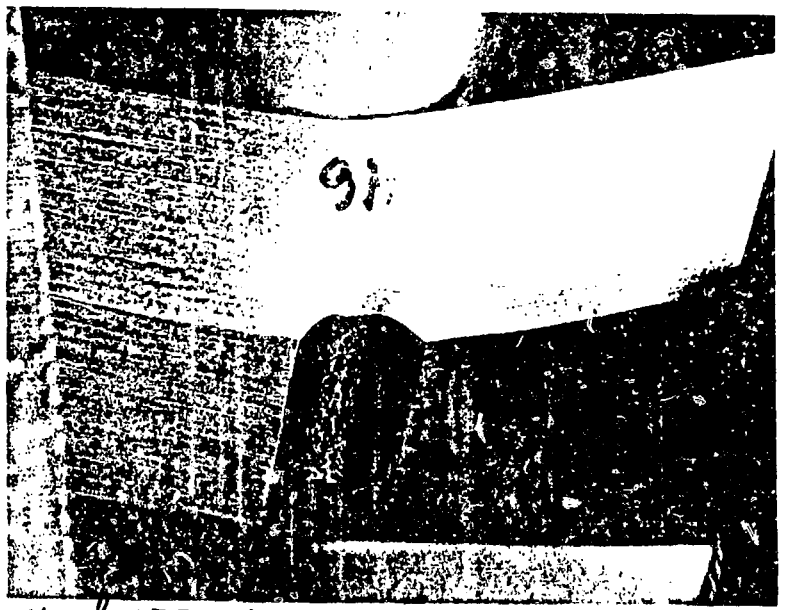

d) at 13.34 KN

Figure 3 Photographic views of slow-bend test of Specimen 38 (0.10 mm notch root radius)

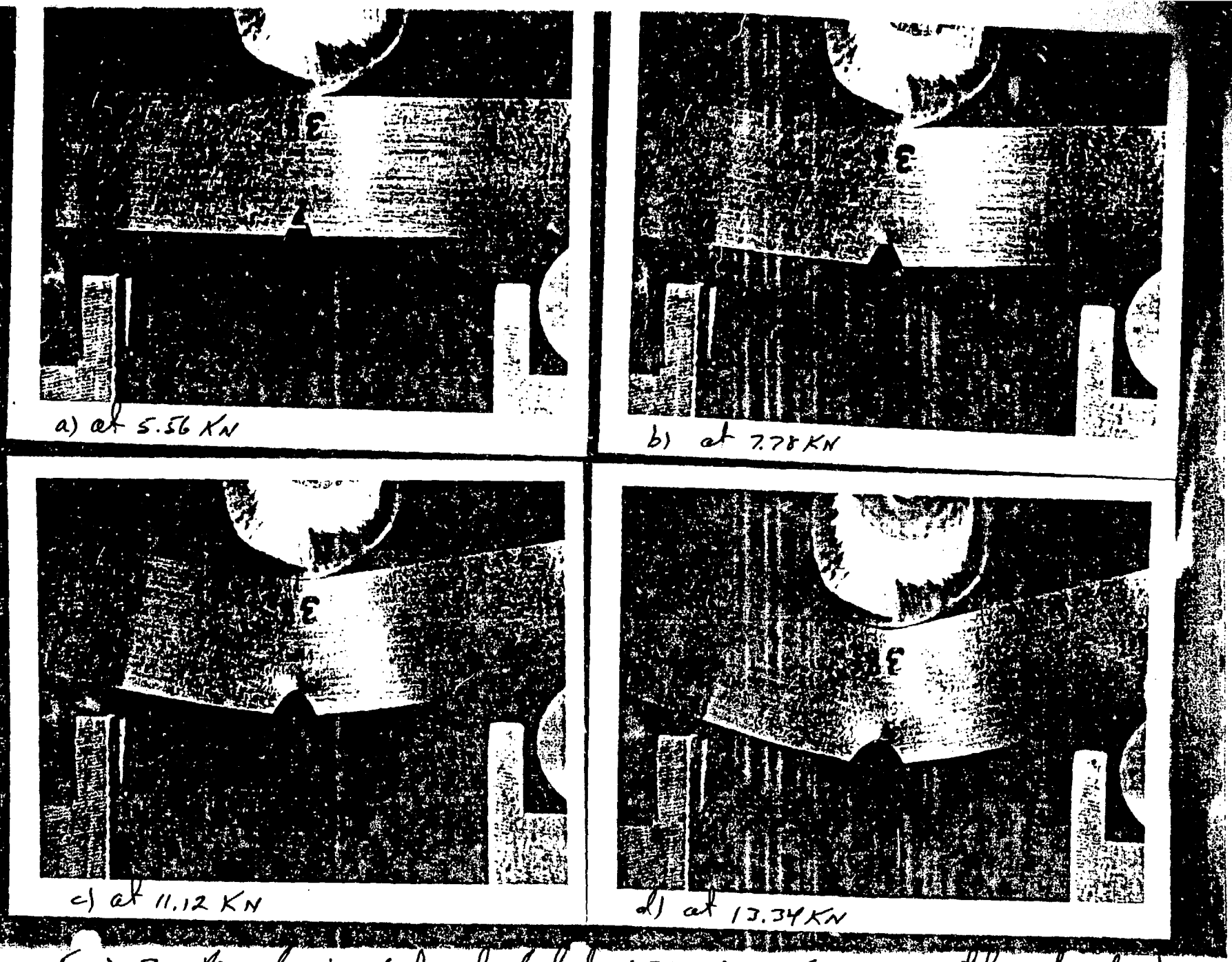

Figure 3 Normal view of slow-bend test of Specimen 38 (0.10 mm notch root radius)

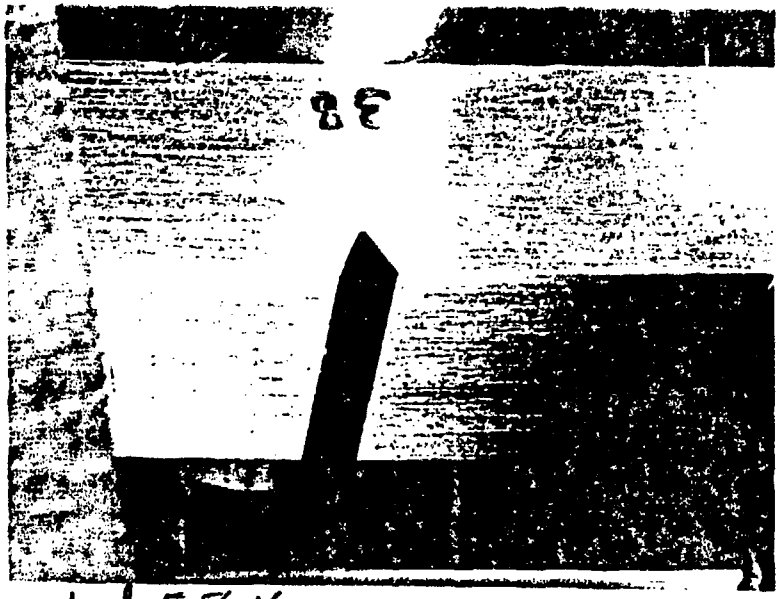

a) at 5.56 KN

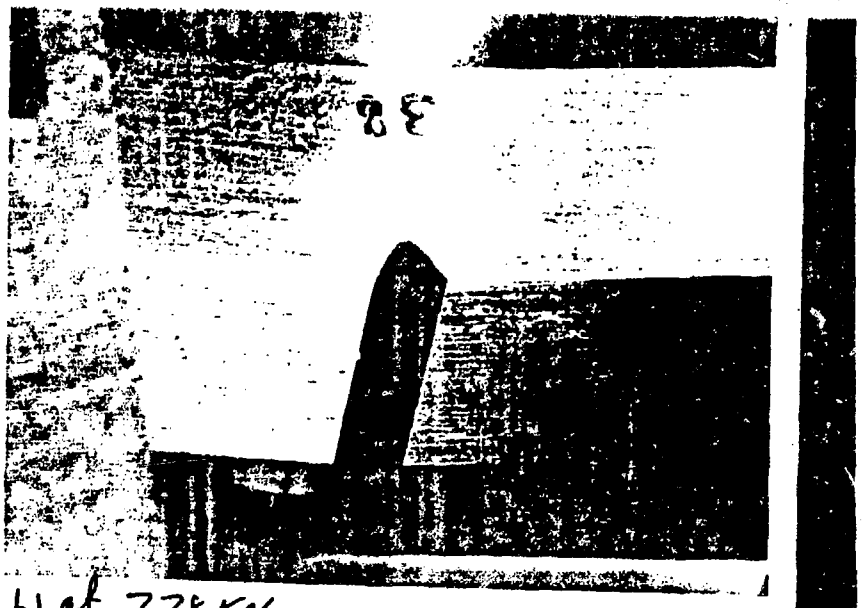

b) at 7.78 KN

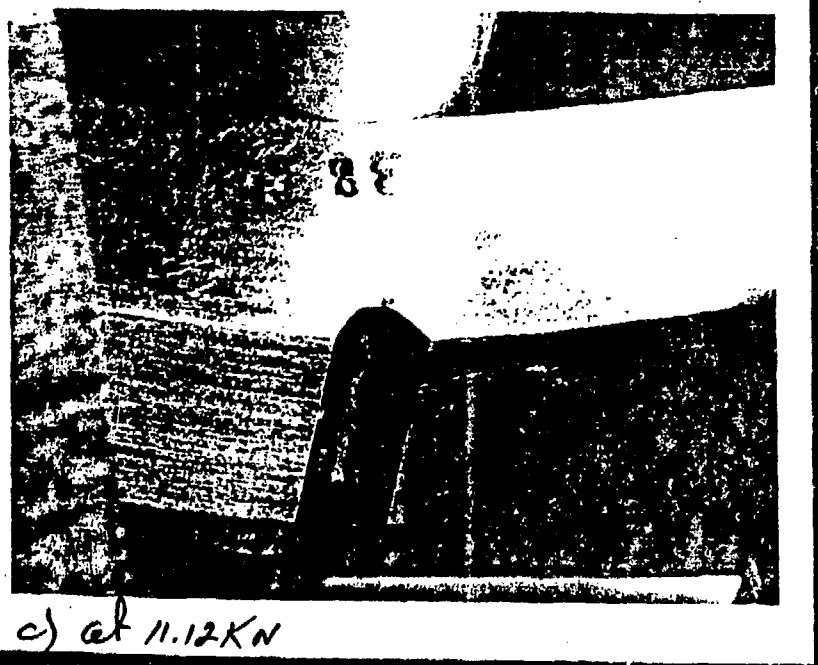

c) at 11.12 KN

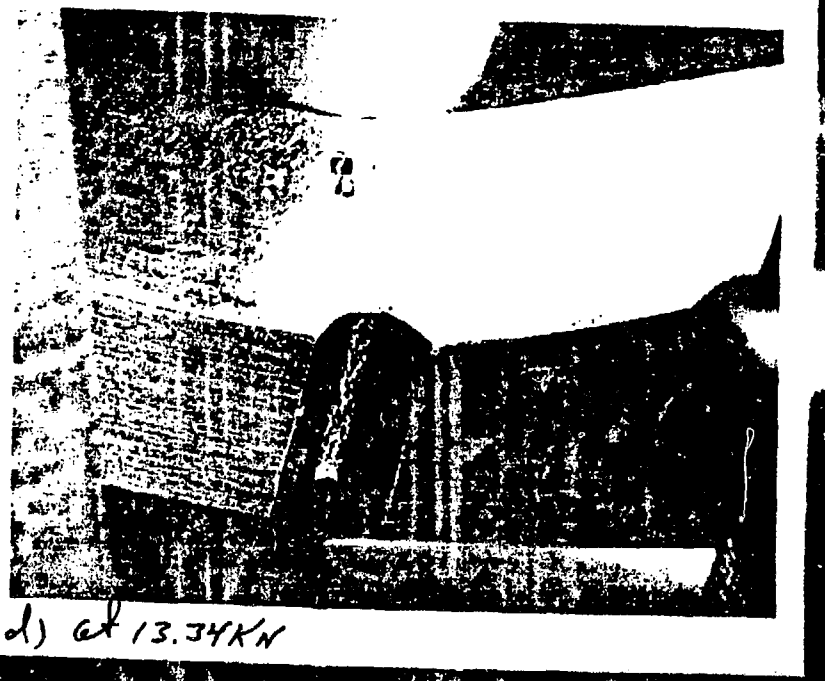

d) at 13.34 KN

Figure 4 Oblique view of slow-bend test of Specimen 38 (0.10 mm notch root radius)

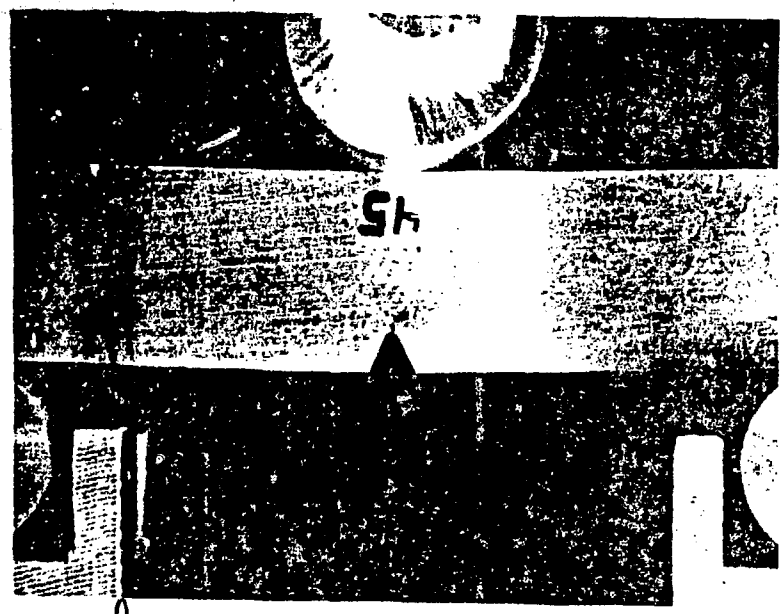

a) at 5.56 KN

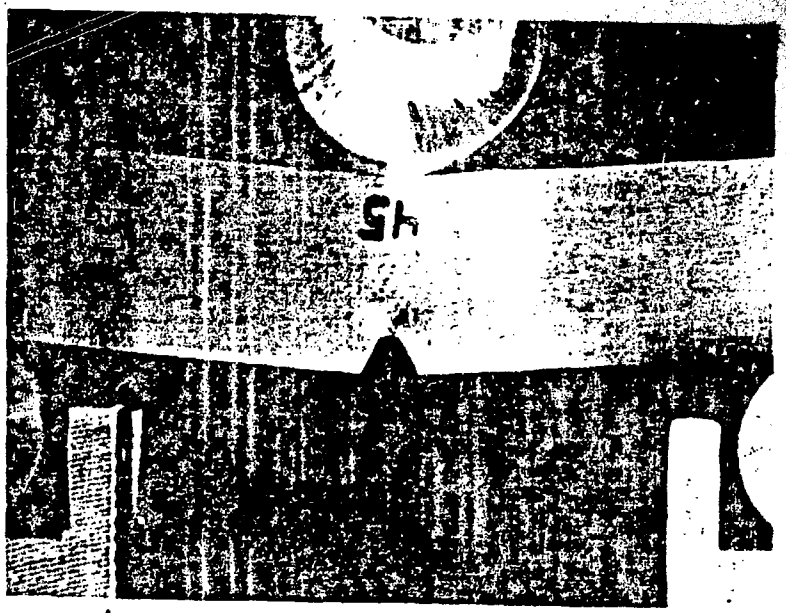

b) at 7.78KN

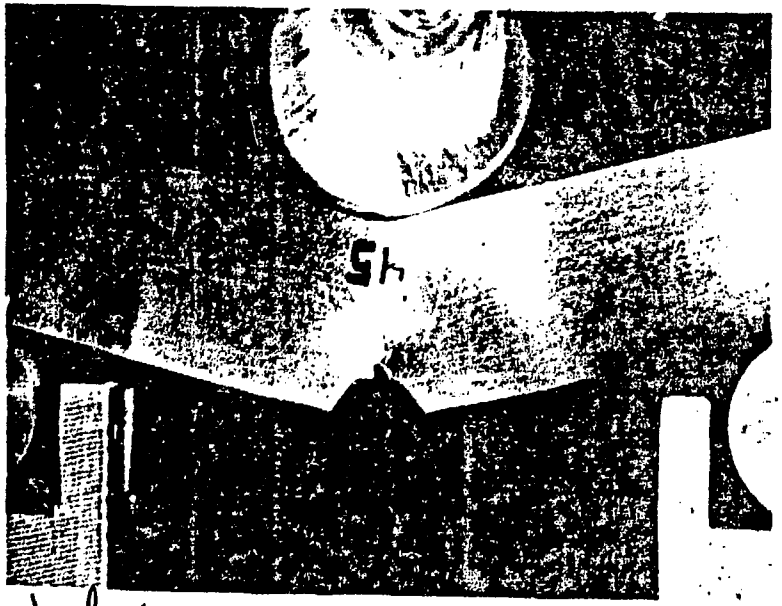

c) at 11.12KN

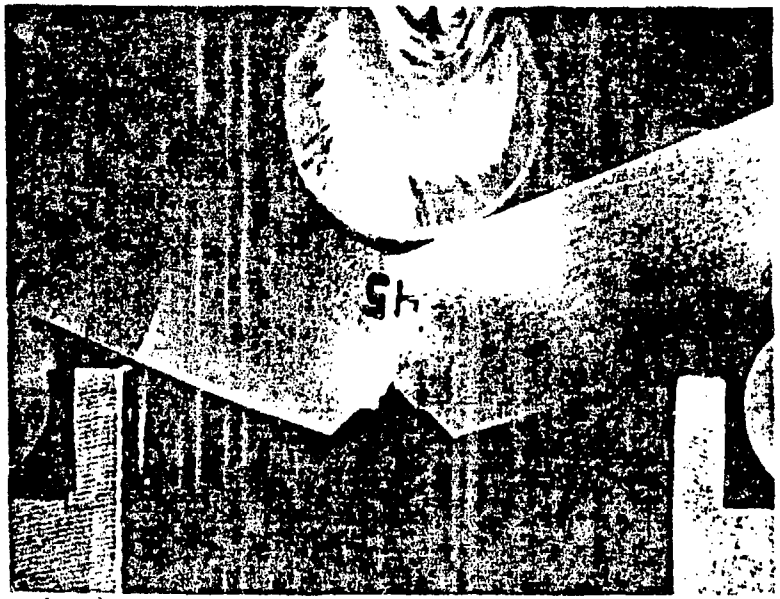

d) at 12.23KN

Figure 5 Normal views of slow-bend test of Specimen 45 (pre cracked, $a/w = 0.23$)

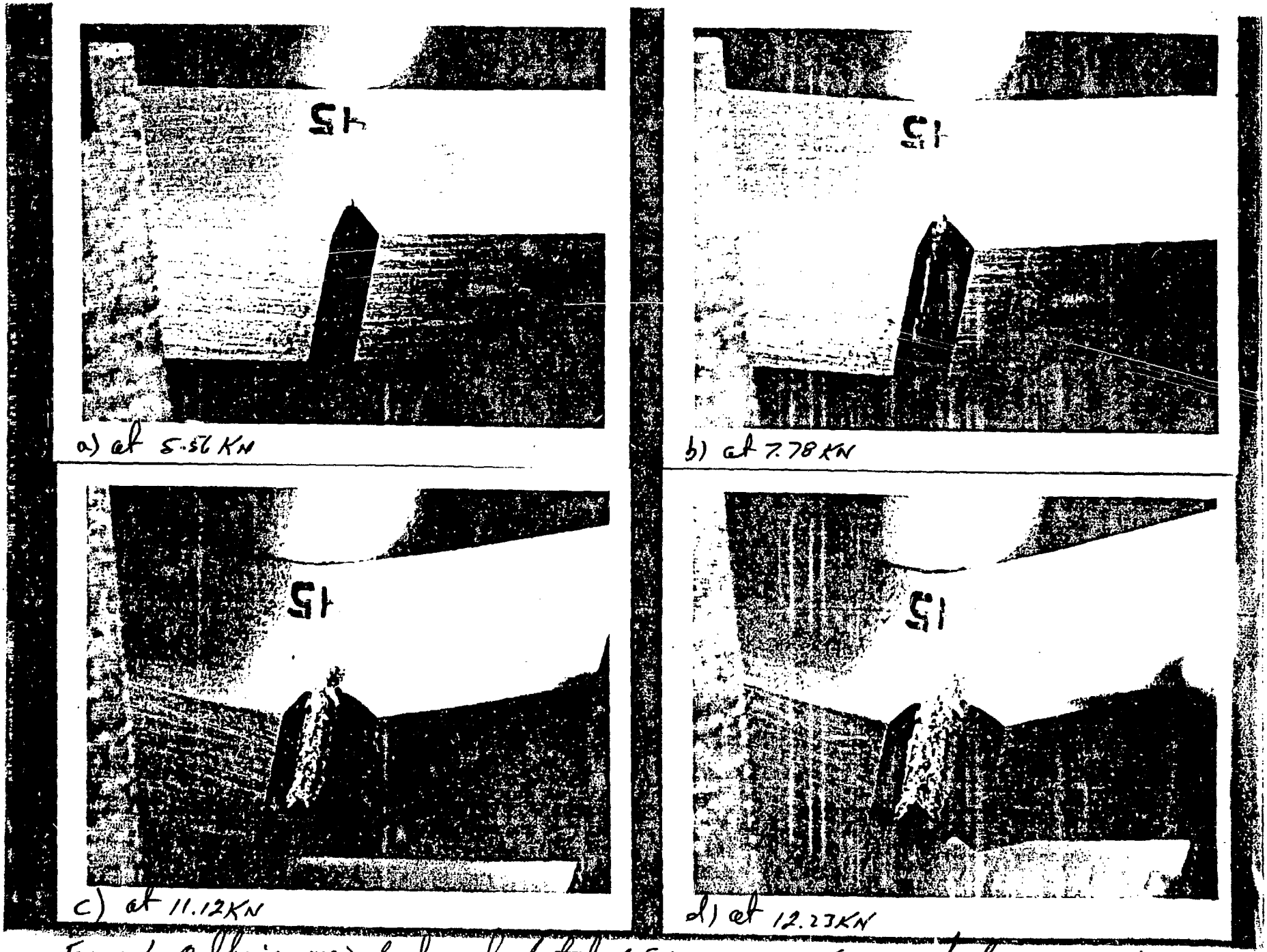

Figure 6 Oblique view of slow-bend test of Specimen 4F5 (precracked, a/w = 0.23)

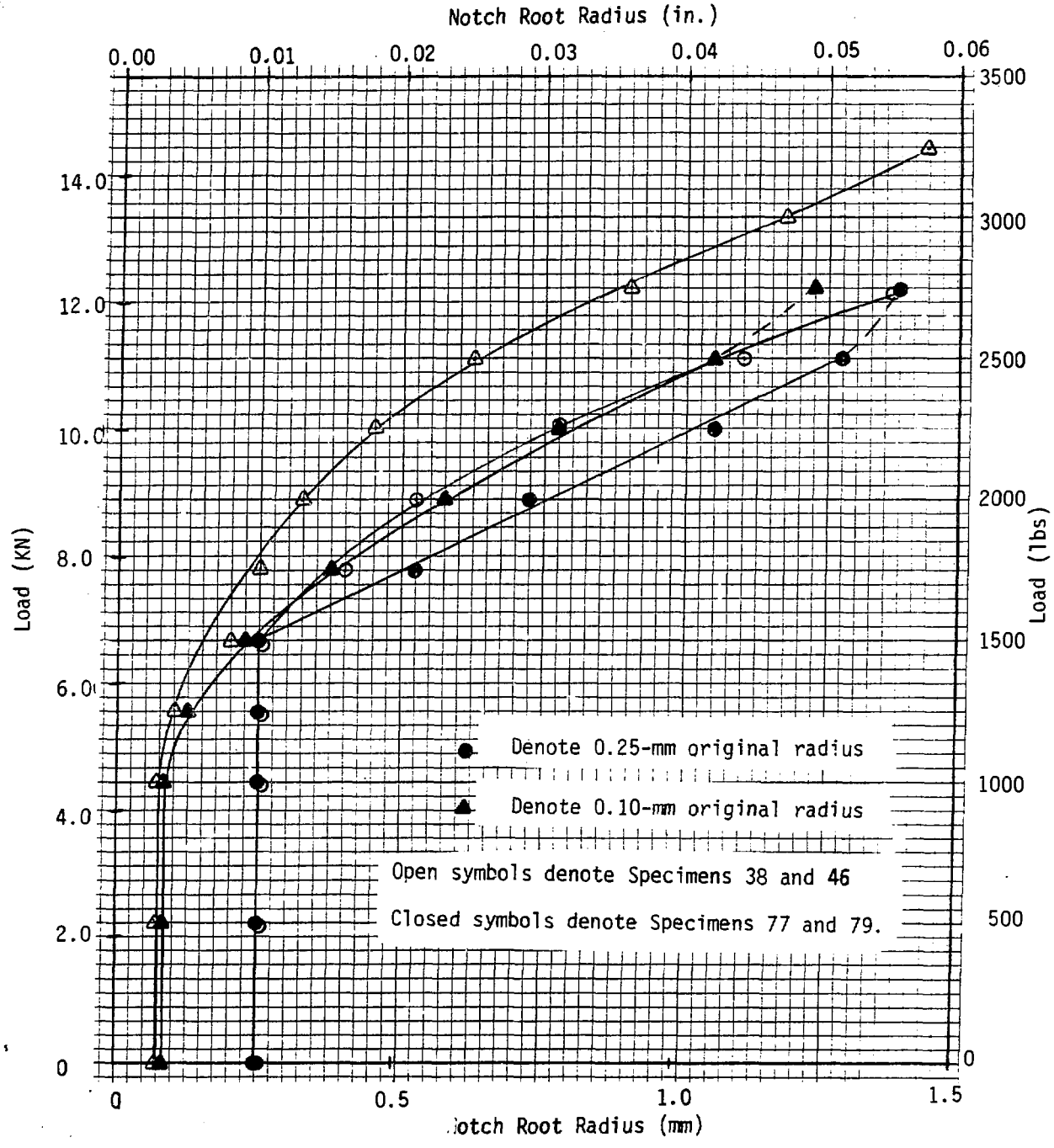
Notch Root Radius (in.)
0.00
0.01
0.02
0.03
0.04
0.05
0.06
Load (KN)
14.0
12.0
10.0
8.0
6.0
4.0
2.0
0
Load (lbs)
3500
3000
2500
2000
1500
1000
500
0
Denote 0.25-mm original radius
Denote 0.10-mm original radius
Open symbols denote Specimens 38 and 46
Closed symbols denote Specimens 77 and 79.
0
0.5
1.0
1.5
Notch Root Radius (mm)

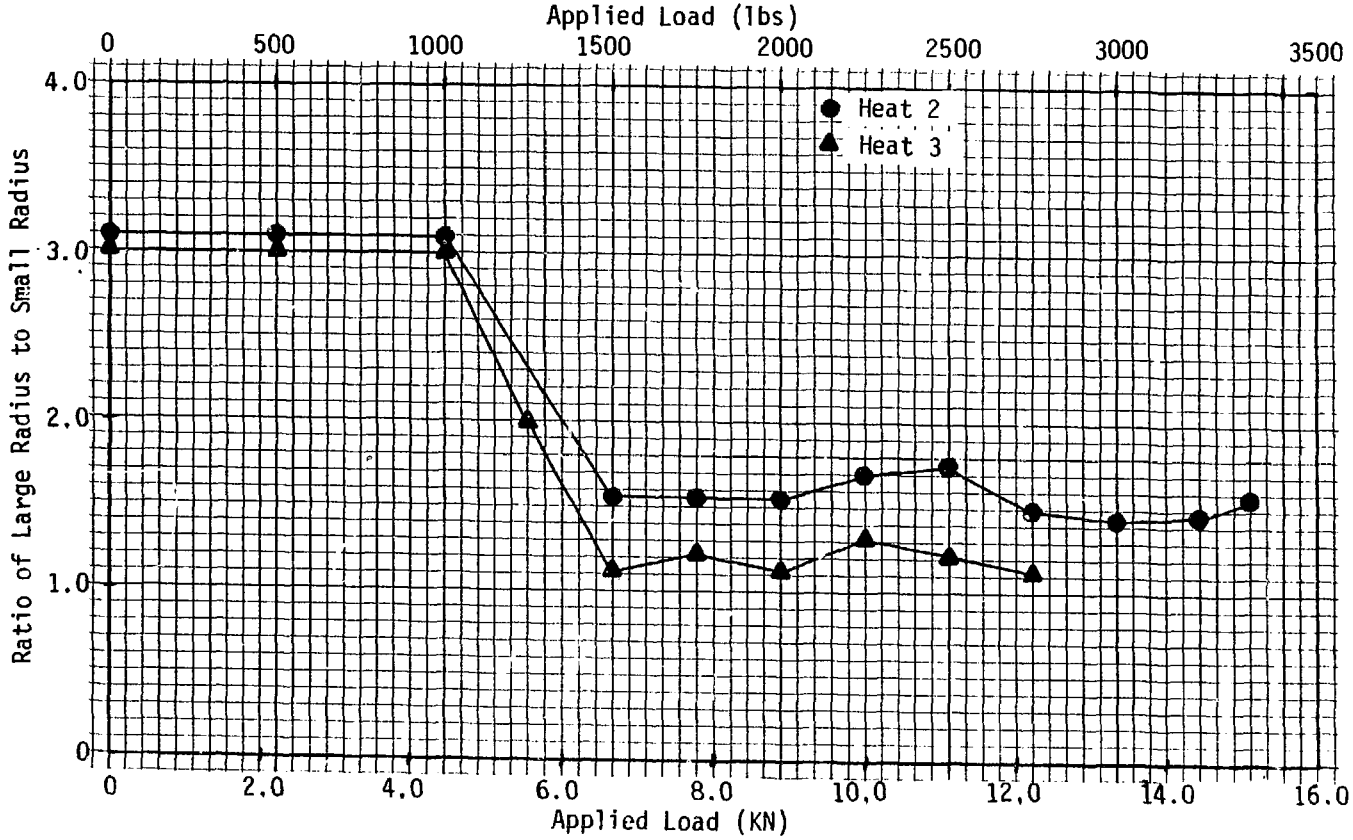
Applied Load (lbs)
0
500
1000
1500
2000
2500
3000
3500
4.0
3.0
2.0
1.0
0
Ratio of Large Radius to Small Radius
Heat 2
Heat 3
0
2.0
4.0
6.0
8.0
10.0
12.0
14.0
16.0
Applied Load (KN)

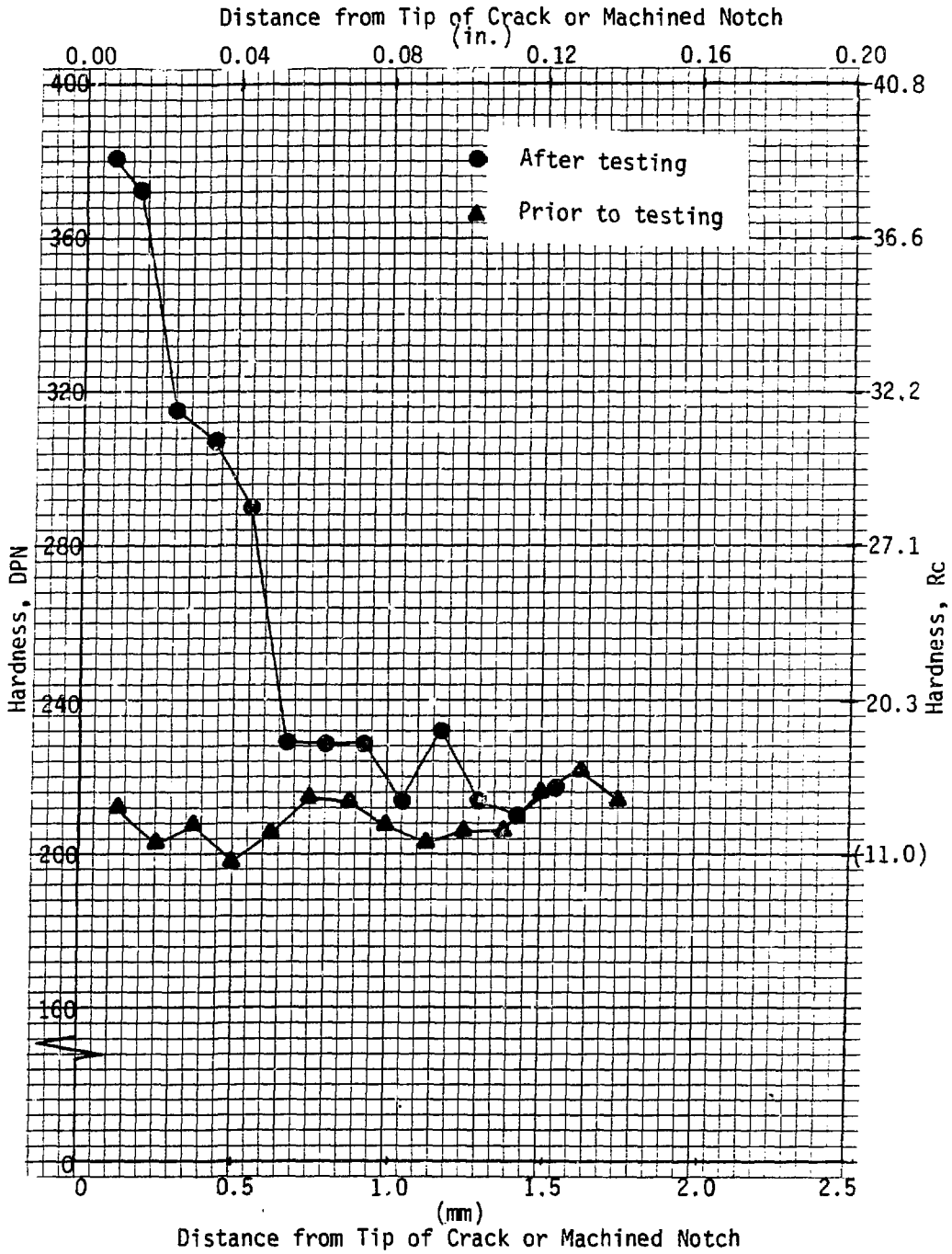
Distance from Tip of Crack or Machined Notch
(in.)
0.00
0.04
0.08
0.12
0.16
0.20
400
360
320
280
240
200
160
0
40.8
36.6
32.2
27.1
20.3
(11.0)
Hardness, DPN
Hardness, Rc
After testing
Prior to testing
0
0.5
1.0
1.5
2.0
2.5
(mm)
Distance from Tip of Crack or Machined Notch

Figure 10 SEM Photographs of the notch tip region for three different specimens.

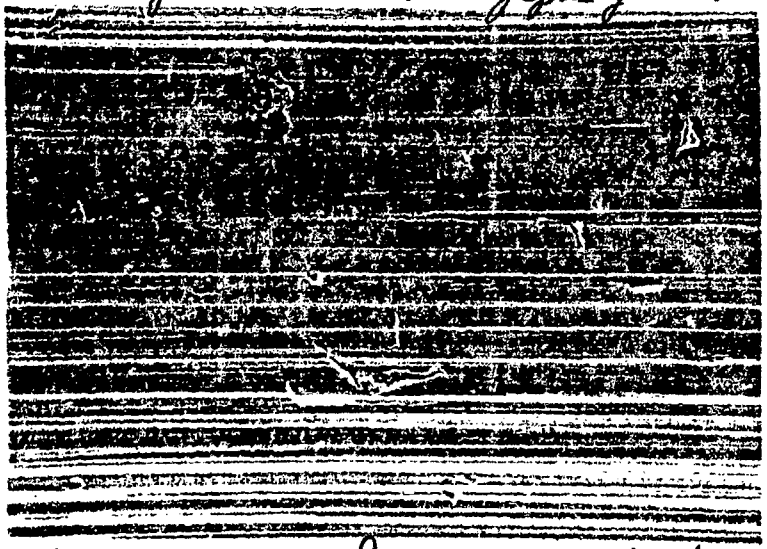

a) Specimen 56 at 70x magnification

b) Specimen 59 at 70x magnification

c) Specimen 59 at 140x magnification

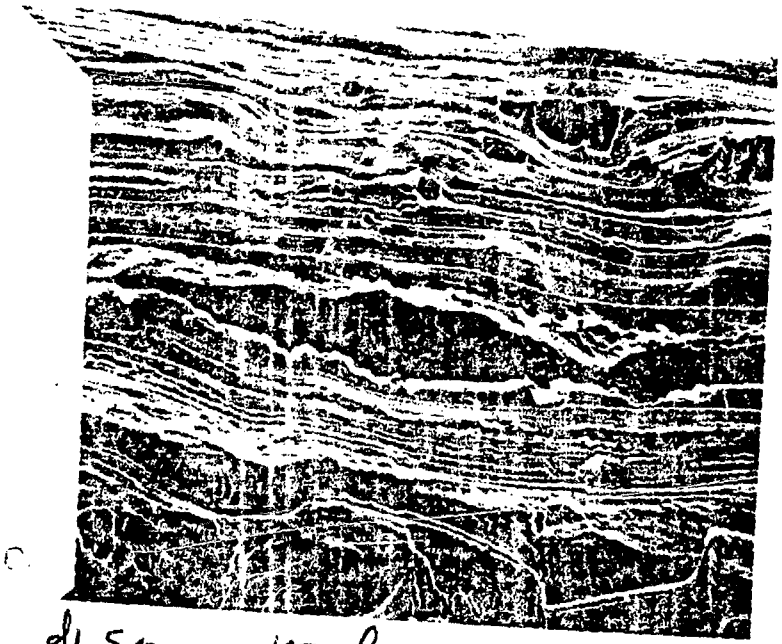

d) Specimen 47 at 70x magnification